Matter

CellPress

Article

# Sequence spinning axially encoded metafibers

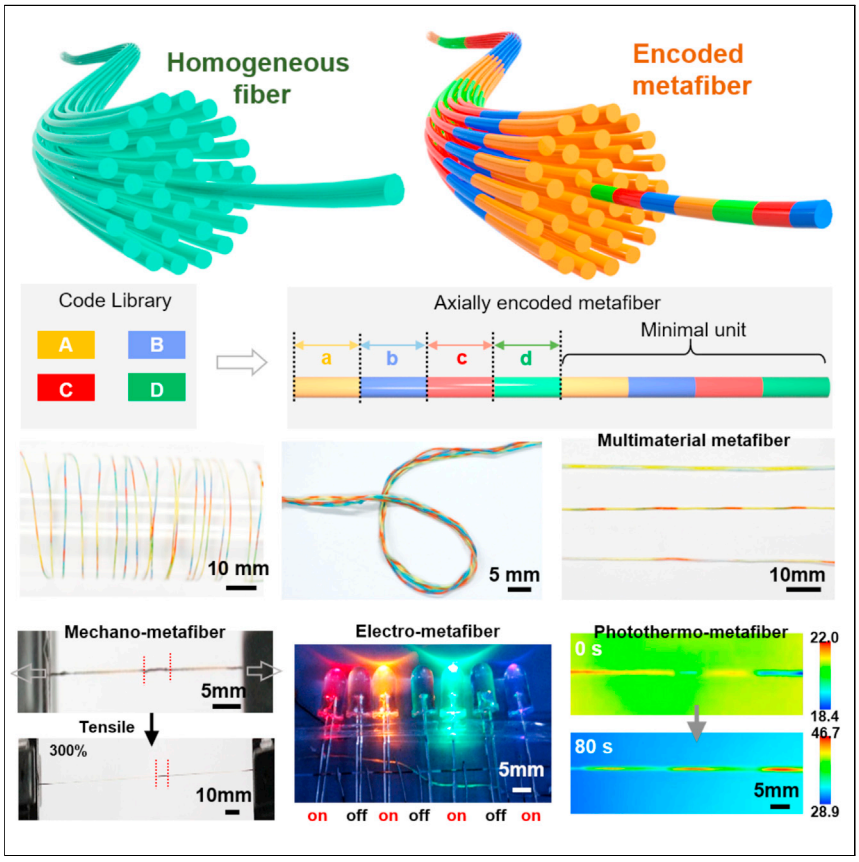


We continuously programmed multiple precisely controlled axial sequencing codes to prepare axially encoded metafibers and multimaterial metafibers with customized axial metastructures by a microfluidic sequence spinning method.

Jingyu Ma, Yingjun Liu, Chao Gao, Zhen Xu

zhenxu@zju.edu.cn

## Highlights

We realized fiber axial asymmetry for designing axially metastructure codes

We extended the concept of axially encoded metamaterials into fibers

We designed a series of unique functional multimaterial metafibers


**Development**

Practical, real world, technological considerations and constraints

Ma et al., Matter 6, 1–16
November 1, 2023 
https://doi.org/10.1016/j.matt.2023.08.006

Please cite this article in press as: Ma et al., Sequence spinning axially encoded metafibers, Matter (2023), https://doi.org/10.1016/j.matt.2023.08.006

Matter

CellPress

Article

# Sequence spinning axially encoded metafibers

Jingyu Ma,[1] Yingjun Liu,[1] Chao Gao,[1] and Zhen Xu[1,2,*]

## SUMMARY

**Fiber, an element component of textiles, biology, and devices, usually features the same composition and functions along its continuous length. Beyond traditional homogeneous structures, fiber has been expected to carry massive metastructure codes with asymmetric properties. Encoding fiber metastructures along the axial direction should reach the maximum code density to design promising axially encoded metamaterial fibers, yet this remains challenging. Here, we continuously program multiple precisely controlled axial sequencing codes in single fiber and prepared axially encoded metafibers by a microfluidic sequence spinning method. The delicate design in axial compositions breaks the fiber symmetry, encoding axially customized metastructures with tunable arrangement and wide material choice for metafibers. We initiated the axially encoded metafiber with asymmetric functions and localized properties to encompass mechanical, electrical, magnetic, and photothermal metafibers. The axially encoded metafiber extends the concept of metamaterials into fiber and fulfills the target demands of future smart textiles.**

## INTRODUCTION

Fiber has evolved from natural to synthetic species, always accompanying human evolution to serve more complex needs.[1] In the information era, fibers are required to carry metastructure codes and functions to construct smart textiles.[1–4] Beyond traditional homogeneous fibers, developing unique fibers with multimaterials to follow the trend of metamaterials can integrate anisotropic customized structural units to possess extraordinary properties.[5,6] For example, integrating asymmetric electrodes and electronic components fabricated fiber electronics, including sensitive stretchable sensors,[7–13] energy harvest,[13,14] energy storage,[15–18] flexible displays,[1,19–24] and information-processing textiles.[5,25,26] The periodically arranged metastructures break the structural symmetry and render metafibers with unprecedented physical (mechanical, optical, etc.) properties that are unavailable in natural or chemically synthesized fibers.[5,6,27,28] Despite many intriguing arranged metastructures being designed in film and monolithic systems, the fibrous form of metamaterials with customized artificial codes waits to be developed.[27,28] To design such metafibers, radial and axial encoding are two basic paths to integrate multimaterials and periodically arranged metastructures in single fiber. Radial encoding has been achieved by switching heterogeneous layers and interfaces through techniques such as post-integration,[9] surface coating,[12,20] coaxial spinning,[8,16] and preform integration.[10,22–24] However, radial encoding theoretically limits the code density, owing to the finite scale. In the other path, axial encoding should render fibers with the maximum code density and more complex functions along the fiber length. This encoding path can fully utilize the ultralong anisotropic profile of continuous fibers and give the vast space to design complex functions for smart textiles. To date,

## PROGRESS AND POTENTIAL

Fiber usually features homogeneous compositions and structures along its length. The development trend of fiber always accompanies human evolution, and fibers are required to carry metastructure codes to construct smart textiles. Beyond traditional homogeneous fibers, developing fibers with axial structural units to possess extraordinary properties needs to be exploited yet still remains a challenge. Here, we continuously fabricate axially encoded metafibers for designing asymmetric functions and localized properties by an automatic microfluidic sequence spinning method. The metafibers have axially encoded multimaterial metastructures, asymmetric functions, and localized properties, encompassing mechanical, electromagnetic, and photothermal species. The axially encoded metafibers extend the metamaterial concept into fibers and expand the multimaterial fiber family, which promises wide uses in smart textiles, such as soft electronics, actuators, sensors, and information delivery.

integrating massive customized metastructure units with designed asymmetry along the fiber axial direction has become a trend yet remains challenging.

Axially encoding metafibers requires accurately integrating compositions in the designed sequences in a continuous manner. Post-treatment of homogeneous fibers has been invented to design local chemical composition and create axial heterostructures. For example, the drop-casting method was used to generate microreactor arrays along the fiber axial direction.[29] Controllable breaking methods in thermal drawing were adopted to design multimaterials as diverse functional units along the fiber axis.[30–32] Apart from the post-treatment techniques, multiphase coaxial microfluidic devices were used to prepare periodic knotted microfibers[33–39] in which the continuous outer sheath wraps separated cores with specific designs. Multichannel microfluidic devices were employed to show the possibility to fabricate segmental microfibers with different luminescence and morphology.[40,41] However, the axially encoded metafibers with metastructures need to be exploited, and how to integrate multimaterials in a continuous manner as axial codes in sequence still remains a challenge.

Here, we continuously fabricate axially encoded metafibers for designing axially asymmetric functions and localized properties by an automatic microfluidic sequence spinning (MSS) method. The MSS method allows precise spatial designing of tunable heterogeneous metastructures and arrangement, fully utilizing the good material processibility of wet spinning and the massive axially asymmetric codes. The axial metafibers feature programmable encoded sequences, and their code density reaches 1,350 per meter along the fiber length. The permutation arrangement of various codes greatly enriches the fiber complexity in short repeating units and extends metafiber categories exponentially in a long axially encoded metafiber. The precise axial encoding and abundance of code arrangement together with wide code choice enable the rich structural design of metafibers. We extend the code type to material categories, morphologies, and functions to exquisitely design a metafiber family with axially customized metastructure units. The metafibers have axially encoded multimaterial metastructures and asymmetric functions and localized properties, encompassing mechanical, electromagnetic, and photothermal species. The axially encoded metafibers extend the metamaterial concept into fibers, expand the multimaterial fiber family, and pave the way to the scalable fabrication of continuous multifunction fibers with axial asymmetry, which promise wide uses in smart textiles, such as soft electronics, actuators, sensors, and information delivery.

## RESULTS AND DISCUSSION

### Spinning axially encoding fiber in MSS system

Conventional fiber is homogeneous along the longitudinal axis; for example, daily commercial nylon, polyester, and acrylic fibers keep consistent composition and morphology along continuous length. As the longitudinal symmetry breaks, homogeneous fibers turn to axially encoded metafibers with customized sequences along the fiber length, enabling a higher code density and axial asymmetry (Figure 1A). We build a mathematical model to precisely describe the encoded metafibers (Figure S1). The fiber can be defined as "$(A_aB_bC_cD_d)_{1/L}$" in mathematics, resembling the nomenclature of a molecular formula. In this definition, A–D represent the material compositions, a–d are the corresponding stoichiometric ratios of each component, and 1/L denotes the linear density of the simplest repeating unit ($A_aB_bC_cD_d$) (Figures 1B and S1). By this model, we expressed the compositions as a function

[1]MOE Key Laboratory of Macromolecular Synthesis and Functionalization, Department of Polymer Science and Engineering, Zhejiang University, 38 Zheda Road, Hangzhou 310027, P.R. China

[2]Lead contact

*Correspondence: zhenxu@zju.edu.cn

https://doi.org/10.1016/j.matt.2023.08.006

Please cite this article in press as: Ma et al., Sequence spinning axially encoded metafibers, Matter (2023), https://doi.org/10.1016/j.matt.2023.08.006





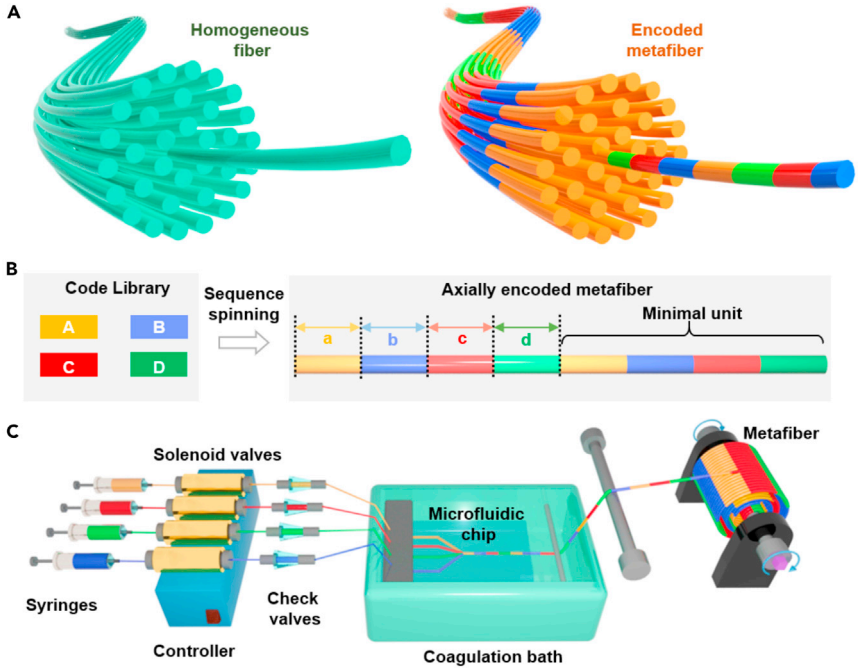


**Figure 1. Schematic illustrations of axially encoded metafibers**

(A) Structural comparison between commercial homogeneous fiber and axially encoded metafiber.

(B) Sequence spinning method of designing the basic unit of the axially encoded metafiber from the code library.

(C) Program-controlled MSS system, which consists of spinning dopes, controller, solenoid valves, check valves, and coagulation bath. The axially encoded metafibers were fabricated by switching the solenoid valves.

Fabrication details are shown in Figures S1 and S2.

of fiber axial direction, converting actual fiber metastructures to quantified mathematical data arrays. We further translated the fiber axis into time variables (Figure S1), which guarantees the axial design of structural sequences under program control.

We set up a program-controlled MSS system to fabricate sequence-encoding metafibers. The mathematical functions of metafibers were realized by the programmable switch of solenoid valves (Figures 1C and S2). During the spinning process, the polyurethane (PU) dopes were selectively injected into the corresponding microfluidic channels and then converged into an outlet, followed by solidification in a coagulation bath (Video S1). The solenoid valves acted as "smart code filters" that open for the designed components and close for the other components, following the program. The selective encoding process was monitored under a microscope (Figure 2A; Video S2). When both valves were open, two spinning dopes in the outlet channel formed lamellar flow (Figure 2B). When the A channel was open and the B channel was closed, the specific "A" sequence in the fiber is encoded (blue, left channel). Switching the state of A and B channels encodes the "B" sequence. Through this control protocol, the sequential spinning of codes in continuous fibers is achieved following the digitally designed program (Figures S3 and S4). The resultant sequence in the final metafiber was examined by pigments and fluorescent tagging (Figure 2C). The independent serial fluorescence along the fiber axis demonstrates that the designed heterogeneous sequences were successfully encoded in a single metafiber to break axial symmetry.

Please cite this article in press as: Ma et al., Sequence spinning axially encoded metafibers, Matter (2023), https://doi.org/10.1016/j.matt.2023.08.006



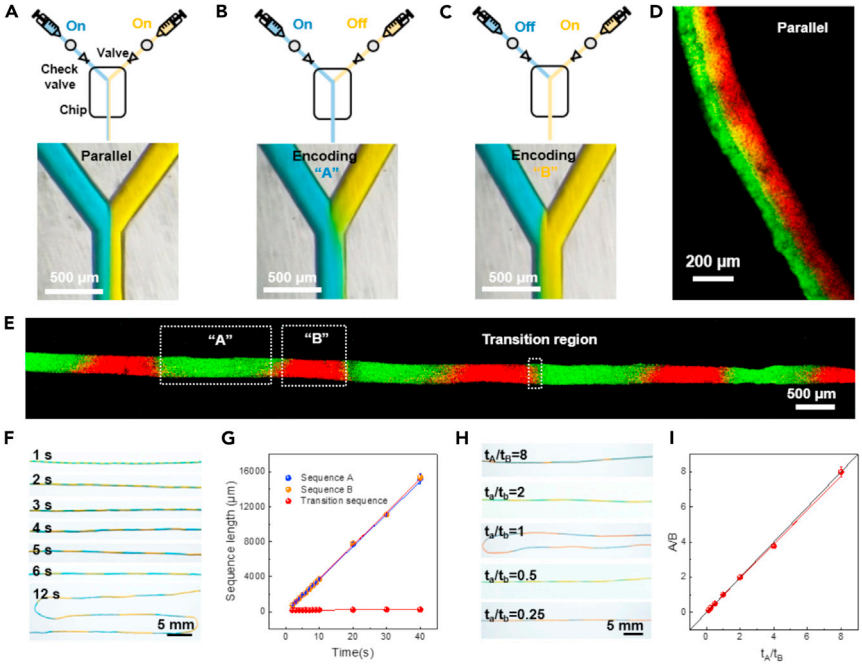


**Figure 2. Axially encoding metafiber sequences**

(A–C) Schematics and digital images of MSS, including three steps: (A) parallel flow and (B) encoding "A" and (C) "B" sequences (from left to right).

(D and E) Fluorescent image of (D) a parallel encoded metafiber and (E) an axially encoded metafiber.

(F) Axially encoded metafibers with various sequence lengths.

(G) Sequence length as a function of valve operation time.

(H) Axially encoded metafibers with various stoichiometric ratios.

(I) Stoichiometric ratio as a function of valve operation time ratio.

Error bars represent the standard deviation of 3 different specimens.

We controlled the code density by tailoring the spinning time and velocity of each sequence. In the spinning procedure, we have

$$F(t) = F(l)\frac{dl}{dv}, \qquad \text{(Equation 1)}$$

where F is the fiber composition and $t$, $l$, and $v$ are the operation time of valve, the length of corresponding sequence, and the spinning velocity, respectively. Provided the constant $v$, $l$ linearly correlates with $t$. Based on this principle, we manipulated the length and stoichiometric ratio by adjusting the spinning time of corresponding sequences (Figures 2D–2G). Importantly, in order to accurately control the sequential length, we placed check valves between the solenoid valves and the microfluidic chip to avoid the reflux caused by the valve shifting (Figures S5 and S6). Owing to the merit of program control, the encoded sequences exhibit good replicability with length statistical variation of less than 3.3% (Figure S7). The highest resolution of $l$ reached 740 μm, and the corresponding maximum sequential code density is 1,350 $m^{-1}$, which is limited by the switching frequency of the valves and controller.

The fiber continuity was ensured by the diffusion between two encoded spinning dopes and the formed tight transition junction. In the microfluidic spinning microchips, the encoded spinning dopes were consistently contacted. The successively encoded spinning dopes underwent interfacial material exchange, leading to a transition region with gradient composition. The existence of transition sequences

Please cite this article in press as: Ma et al., Sequence spinning axially encoded metafibers, Matter (2023), https://doi.org/10.1016/j.matt.2023.08.006





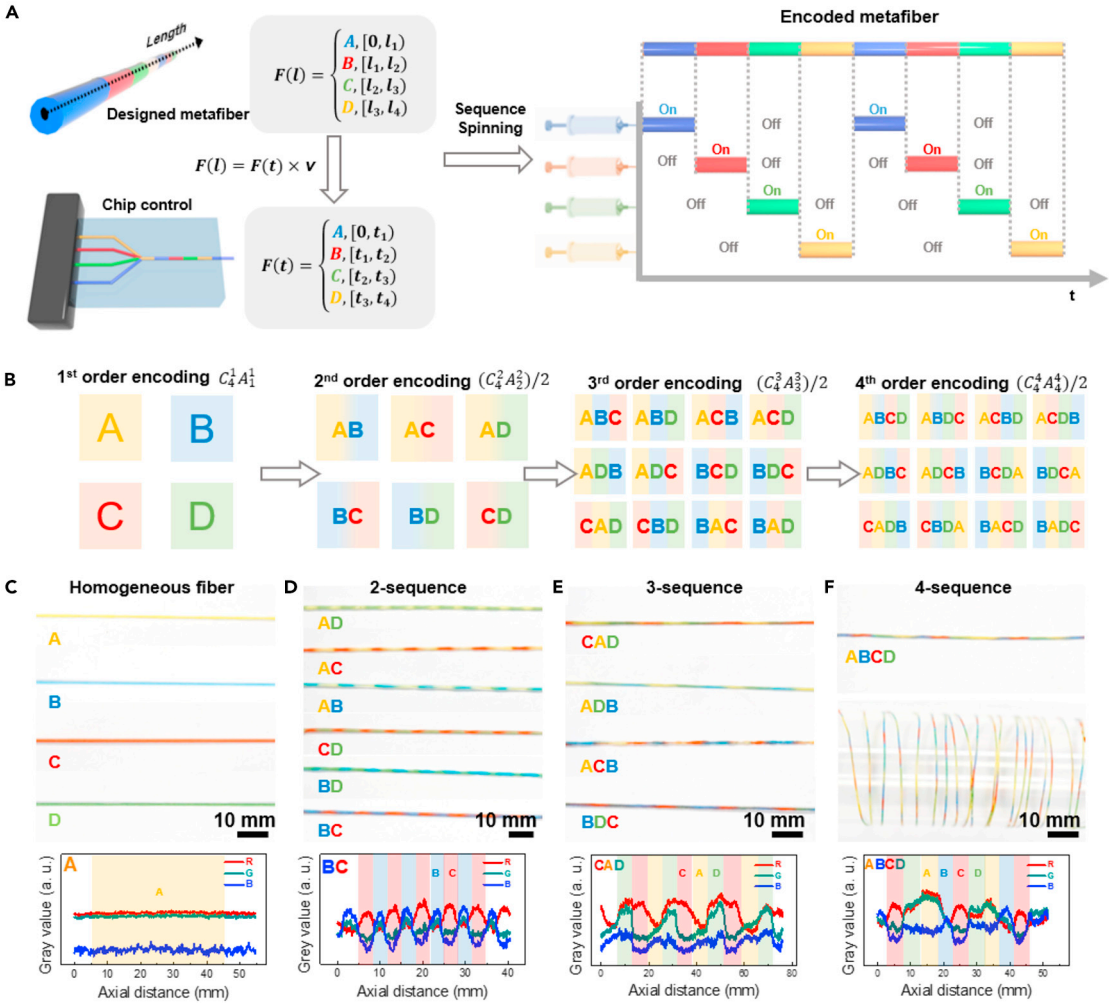


**Figure 3. Permutation arrangement of axially encoded metafibers**

(A) Schematics of designing encoded metafibers with multiple sequences.

(B) Schematics of encoding process of metafibers with multiple sequences.

(C) Images of homogeneous fibers and gray-value analysis of a neat "A" fiber.

(D) Two-sequence encoded metafibers and gray-value analysis of a "BC" metafiber.

(E) Three-sequence encoded metafibers and gray-value analysis of a "CAD" metafiber.

(F) Four-sequence encoded metafibers and gray-value analysis of a "ABCD" metafiber.

was confirmed by fluorescent optical microscopy (Figures 2C and S4). The width of the transition sequences remained unchanged at different spinning times and linearly correlated with spinning velocity (Figure S8). For example, when $v$ is 2 μL $min^{-1}$ and $t$ is 5 s, the transition regions account for 4.3% of all the sequence length, which is negligible in designing axially encoded metafibers.

## Permutation arrangement of encoded sequences

We extended the code complexity to higher orders by increasing the code types in one minimal unit. Adopting a 4-channel MSS system, we demonstrated the exquisitely designed permutation arrangement of encoded sequences by successive encoding spinning programs (Figure 3A). Starting with a single code, we sequentially encoded different codes step by step to prepare multicode metafiber in 4 orders (Figure 3B). We used different pigments to label codes, and the designed

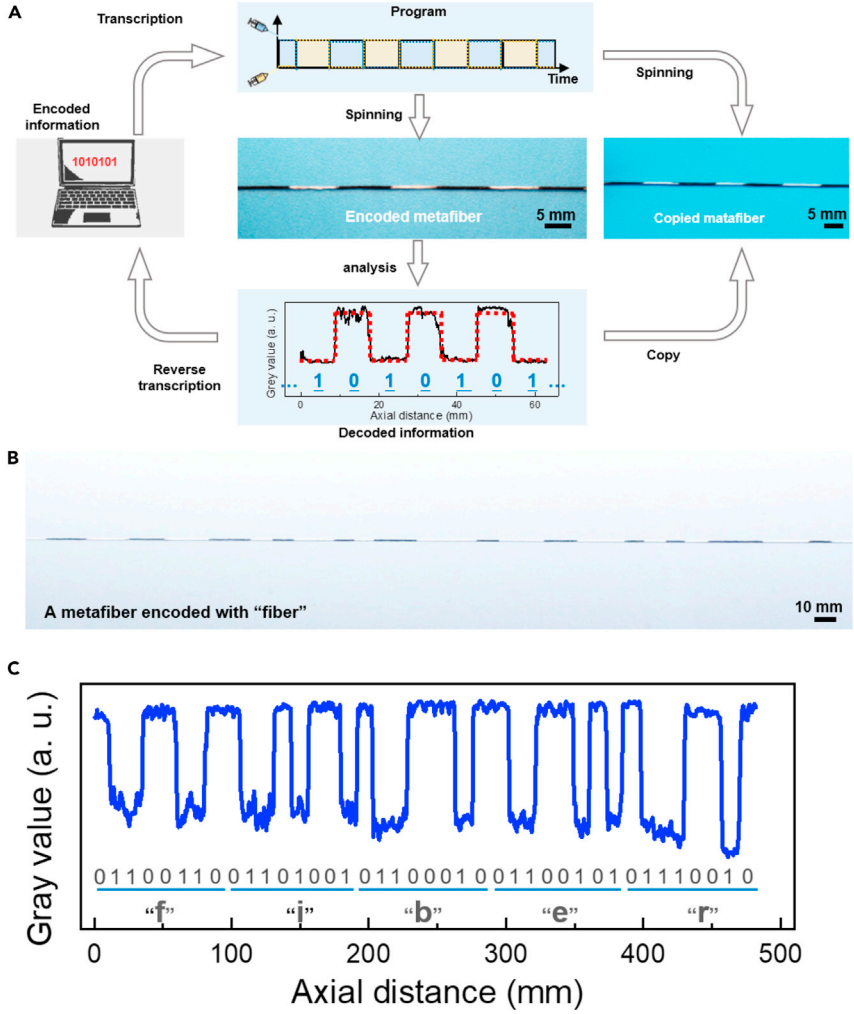


**Figure 4. Encoding and decoding of metafibers**

(A) Procedures of encoding and decoding information in metafibers.

(B) A metafiber encoded with word "fiber."

(C) Axial gray-value analysis of the encoded metafiber.

Related design programs are shown in Figure S10.

fiber units were confirmed by detailed gray analysis (Figures 3C–3F). The metafiber complexity increases as the code order increases, following the combined probability principle. In the 1-order case, 4 encoded fiber units with homogeneous axial sequences were obtained, and the combined number can be calculated as $C_4^1$. As the combination order increases from 2 to 4 orders, the complexity increases from 6 ($\frac{1}{2}C_4^2A_2^2$) to 12 ($\frac{1}{2}C_4^4A_4^4$), greatly enriching the code library of metafiber.

## Encoding and decoding information in metafibers

We realized the encoding and decoding of information in a long single metafiber, mimicking the DNA transcription mechanism. We only used 2 codes, which are black graphene-mixed PU (set as 0) and white $TiO_2$-mixed PU (set as 1), to design abundant digital information in one fiber (Figure S9). Taking an information code "1010101" as an example, we first transferred the designed code into the spinning program, which was defined as the "transcription" process to mimic the information encoding of DNA (Figures 4A and S10). Then, the metafiber with the required

Please cite this article in press as: Ma et al., Sequence spinning axially encoded metafibers, Matter (2023), https://doi.org/10.1016/j.matt.2023.08.006





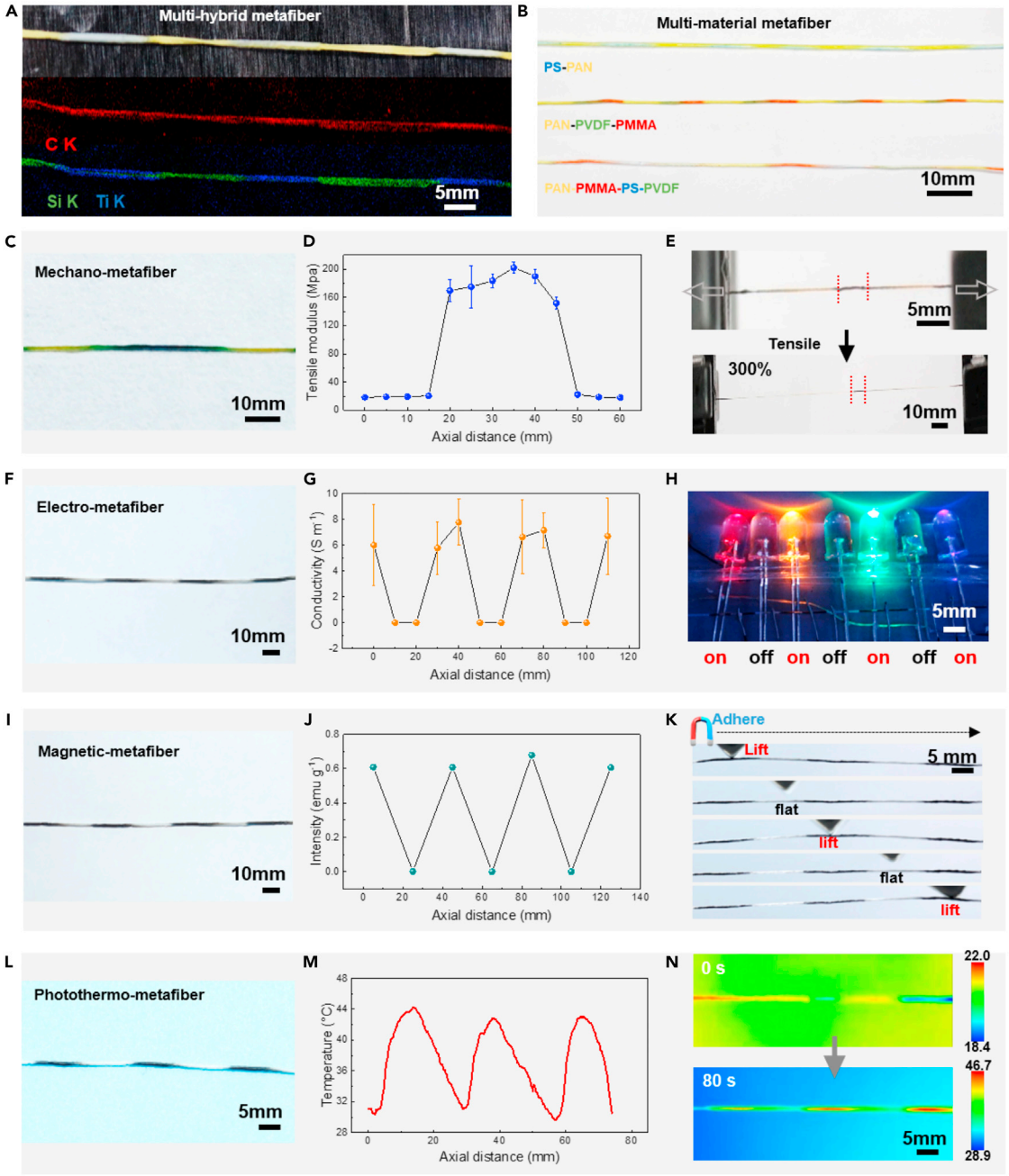


**Figure 5. Multimaterial and multifunction metafibers**

(A) Images and elemental mapping of a multihybrid metafiber.
(B) Multimaterial metafibers.
(C) A mechano-metafiber.
(D) Tensile modulus as a function of mechano-metafiber axial distance.
(E) Localized deformation of the mechano-metafiber under homogeneous axial stress.
(F) An electro-metafiber.
(G) Conductivity as a function of electro-metafiber axial distance.
(H) Localized conductivity of the electro-metafiber. Each sequence was connected to a LED lamp.
(I) A magnetic metafiber.
(J) Magnetization as a function of magnetic metafiber axial distance under a magnetic field of 1 T.
(K) Localized response of the magnetic metafiber under a magnet.
(L) A photothermo-metafiber.

Please cite this article in press as: Ma et al., Sequence spinning axially encoded metafibers, Matter (2023), https://doi.org/10.1016/j.matt.2023.08.006



**Figure 5. *Continued***
(M) Temperature as a function of photothermo-metafiber axial distance under an infrared lamp for 80 s
(N) Infrared images of the photothermo-metafiber under an infrared lamp.
Error bars represent the standard deviation of 3 different specimens. The detailed data of mechano-metafibers, electro-metafibers, magnetic metafibers, and photothermo-metafibers are shown in Figures S15–26, respectively.

encoded sequences was prepared by sequence spinning corresponding codes following the designed program. Decoding metafibers was realized by gray-value analysis to read the encoded information. As shown in Figure 4A, the gray-value evolution along the axial direction represents the sequential code distribution. The decoded gray-value curve was further converted to information code and used as the program to fabricate another metafibers, similar to the "reverse transcription" and "copy" processes of RNA. Based on this concept, we revealed that MSS metafibers were capable of storing and delivering digital information. We increased the codes to encode words in a long single metafiber (length of 480 mm) by binary coding system (Figures 4B and 4C). Every 8 adjacent codes were defined as a letter according to the ASCII coding system, and 40 codes were encoded to form the word "fiber," which shows the possibility of communication by encoded metafibers.

## Encoding multicomposition metafibers

We enriched the code type to material compositions to synthesize a library of metafibers with diverse morphology, hybrids, and materials. The metastructure codes with diverse forms render metafibers with customized composition asymmetry. For multimorphology design, we programmed axial morphologies by encoding spinning dopes with different solid content of spinning dopes to form spindle-shaped and sickle-shaped metafibers (Figure S11). In a multihybrid system, we chose PU as the fiber matrix and different functional nanoparticles as the hybrid agents. Encoding hybrid spinning dopes realized the programmable hybridizing metafiber axially and kept the fiber continuity because of the chemical compatibility between the adjacent fiber sequence matrix. The functional nanoparticles $SiO_2$-hybrid PU (yellow) and $TiO_2$-hybrid PU (blue) were alternatively introduced into successive sequences to prepare a multihybrid metafiber (Figure 5A). Element mapping in scanning electron microscopy (SEM) indicated the hybridization of the corresponding sequences independently while keeping continuity.

For the first time, we created a library of multimaterial encoded metafibers by MSS, including 10 kinds of materials (Figures 5B and S12–S14; Table S1). The library includes the arrangement of hydrophilic polymers (e.g., polyacrylamide, sodium polyacrylate), hydrophobic polymers (e.g., polyacrylonitrile, polyvinylidene fluoride), and inorganic graphene oxide (GO). We carefully chose the spinning system to prepare continuous multimaterial metafibers considering the chemical compatibility. By designing the axially encoded multicomposition metafibers, we revealed that such "block" metafibers can be prepared in one step by directly wet spinning. The combination of multimaterial integration and periodically arranged metastructure expands the metamaterial metafiber family and brings more exotic functions.

The encoded metafibers have alternatively customized metastructures to overcome the challenge of designing axially metamaterial fibers. The reported methods including preform designing,[10,22–24] controllable breaking,[30–32] and multiphase microfluidic spinning,[33–39] only focused on designing axially knotted fibers. The structure of such knotted fibers is axially distributed cores wrapped by a continuous

Please cite this article in press as: Ma et al., Sequence spinning axially encoded metafibers, Matter (2023), https://doi.org/10.1016/j.matt.2023.08.006





sheath along the fiber length direction, which means that the fiber still possesses axial symmetry with homogeneous properties considering the sheath materials. Therefore, breaking fiber axial symmetry is the key limitation for designing multimaterial metafibers with periodically arranged heterogeneous metastructures. As a comparison, our axially encoded metafibers possess several advantages: (1) precise control of the axial segmental compositions rather than sheath-wrapped-core structures, (2) wide material choices and tunable arrangement for the multimaterial and metastructure integration, and (3) the advantage of encoding axial asymmetry. Thus, the sequentially encoded multimaterial metastructures break the fiber axial symmetry, leading to localized heterogeneity. The precise, diverse arrangement, wide material choices, and axial asymmetry of encoded metafibers break through the limitation of axially designing fibrous metamaterials.

## Mechano-metafibers

We designed metafibers with mechanical sequences, coined as mechano-metafibers, by alternatively encoding soft and stiff sequences along the axial direction. We introduced two types of PU with varied mechanical properties into a continuous metafiber successively (Figure 5C). The tensile modulus of the blue sequence (stiff PU) is around 10 times of the yellow sequence (soft PU), indicating the varied axial mechanical properties (Figures 5D and S15–S17). The encoded material asymmetry of mechano-metafiber breaks the mechanical symmetry, realizing the fiber form of the mechanical metamaterial. Different from homogeneous fibers, the mechano-metafiber exhibited a typical localized deformation behavior under homogeneous axial stress because of mechanical asymmetry. Upon stretching, the stiff sequences acted as rigid points with little deformation, while the soft sequences worked as weak points where the tensile strain was greatly expressed (Figures 5E, S18, and S19; Video S3). Under tension, the soft part can exhibit around 11 times the strain of the stiff sequences, representing a complex non-linear deformation mode. This artificial deformation behavior of mechano-metafibers mimics natural soft materials to carry periodically arranged metastructures for mechanical asymmetry.[42–44] The programmable and localized mechanical properties conferred the metafibers with diverse functions, such as designed mechanical properties,[45,46] bridge-island structures,[47] and strain amplifier,[45] which possess great potential in highly sensitive sensors, wearable electronics, and smart actuation.

## Electro-metafibers and magnetic metafibers

The integration of periodic arranged customized metastructure codes with diverse electrical and magnetic properties generated electro-metafibers and magnetic metafibers. We designed graphene-hybrid PU as conductive codes (6.13 S $m^{-1}$) and neat PU as insulative ones (Figures 5F, 5G, and S20). The encoded conductive sequences were separated by the insulating PU sequences, forming repeating electrode-dielectric layer structures. We designed a circuit, and each sequence was connected to an LED lamp (Figures 5H and S21). When applying a voltage as high as 5 V, the LED lamps connected to the conductive sequences were turned on, whereas the insulating ones were off, showing the selective conductivity in corresponding encoded sequences. The electro-metafiber exhibited selective response in conductive sequences under homogeneous tensile strain and worked as a localized sensor (Figure S22). In the magnetic metafiber, $Fe_3O_4$-hybrid PU was designed to be ferromagnetic codes and $Al_2O_3$-hybrid PU to be diamagnetic ones. The varied axial magnetization was confirmed by the magnetization curves (Figures 5I, IJ, and S23). The localized ferromagnetism endows localized response under an exerted magnetic field (Figure 5K; Video S4). The ferromagnetic sequences

Please cite this article in press as: Ma et al., Sequence spinning axially encoded metafibers, Matter (2023), https://doi.org/10.1016/j.matt.2023.08.006



were quickly lifted up as soon as they put close to a magnet, while the diamagnetic parts showed no response and remained flat.

## Photothermo-metafibers

We fabricated photothermo-metafibers by encoding graphene-hybrid PU (infrared absorber) and $TiO_2$-hybrid PU (infrared reflector) to achieve a localized photothermal response in one single fiber (Figures 5L, S24, and S25). Under infrared (IR) exposure, the axial absorption variation spontaneously triggered the localized temperature increase. We used an IR camera to capture the temperature distribution along the fiber axial direction (Video S5). The photothermo-metafiber showed homogeneous temperature distribution at the ambient condition (Figure S26). When exposed under an IR lamp (100 W, 40 cm), the graphene active sequences quickly absorbed radiation, leading to a fast temperature increase (20 K within 80 s). On the contrary, the $TiO_2$ sequences exhibited a slow temperature increase (7.5 K within 80 s) because of the IR reflection (Figures 5M and 5N). The alternative arrangement of the two sequences generated a localized temperature gradient, which may have applications in physical therapy[2] and thermoelectric textiles.[48]

## Axially encoded metafibers for textiles

We used automatic MSS to directly prepare metafibers with axially heterogeneous compositions on a large scale. MSS allowed fabricating single metafibers, metafiber bundles, and metafiber rolls (Figures 6A–6C). The obtained metafibers were continuous and kept intact when being stretched, looped, and even twisted (Figures 6D–6F), enabling the fabrication of freestanding nets and textiles (Figures 6G–6I). Commercial cotton was encoded in two dimensions by simply weaving our metafibers both in rows and columns. The independent metafiber sequence (around 4 mm) was identified as a single code, which represented the basic unit of the "fiber matrix." As shown in Figure 6J, electro-metafibers with 4 sequences were woven into the cotton to form a "4 × 4" network. The conductive sequences (black) were set as "1," and the insulating sequences were set as "0." We defined the matrix operation as the sum up of the multiples of adjacent code in a single rectangle,

$$c_{ij} = a_{ij}b_{ij} + a_{ij}b_{i(j+1)} + a_{(i+1)j}b_{ij} + a_{(i+1)j}b_{i(j+1)}, \quad \text{(Equation 2)}$$

where $a$, $b$, and $c$ are the elements in the row, the column, and the calculated matrix, respectively. $i$ and $j$ are the row and the column of the elements that appear in the matrix. The value of calculated $c_{ij}$ demonstrates the number of conductive paths (0, 1, 2, 4) through the diagonals of the fiber rectangle (Figure S27). The calculated matrix fitted the experiment results as the LED lamps were turned on at the position of the conductive units (Figures 6K and S27). We also integrated one single magnetic metafiber into the cotton to fabricate a magnetic clip that clamped at the ferromagnetic region under the actuation of a magnet (Figures 6L and S28), elaborating the potential in soft robotics with programmed magnetic-field-driven actuation.[49,50]

## Conclusion

In this work, we developed a versatile MSS technique to precisely encode fibers in the axial direction and produced metastructured fibers. The axially coded metafibers have a wide material choice in the code sequence and feature rationally designed axial asymmetry. The sequence spinning method allows arbitrarily designing code arrangement and extends code form to morphology, material compositions, and sequence properties, which greatly enriches the categories of multimaterial and metamaterial metafibers. The customized encoded metastructures of metafibers feature asymmetric functions and localized properties, opening a broader room to design fibrous materials starting from the basic single fiber. The automation also

Please cite this article in press as: Ma et al., Sequence spinning axially encoded metafibers, Matter (2023), https://doi.org/10.1016/j.matt.2023.08.006



CellPress

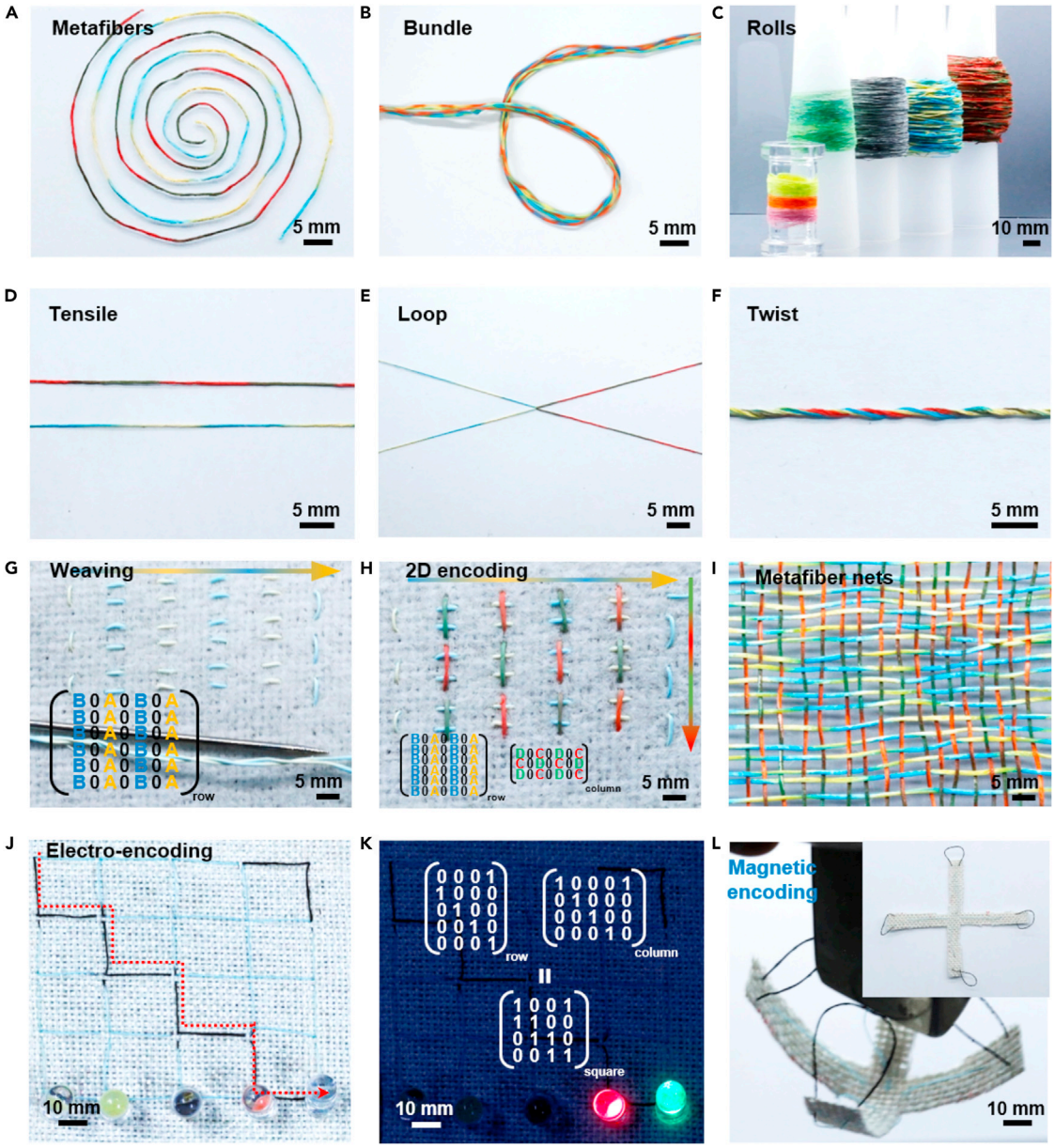


**Figure 6. Axially encoded metafibers for textiles**

(A) Digital images of metafibers.
(B) A bundle of metafibers.
(C) Metafiber rolls.
(D) Tensiled metafibers.
(E) Looped metafibers.
(F) Twisted metafibers.
(G) 1D woven metafibers; inset is the fiber matrix used to describe the encoded information.
(H) 2D encoded metafibers by warp and weft weaving.
(I) Metafiber nets.
(J) 2D encoded electro-metafibers; the black sequences are conductive, forming a zigzag conductive path.
(K) 2D encoded electro-metafibers under a 5 V voltage.
(L) A magnetic clamp prepared by weaving a single magnetic metafiber into the commercial cotton.
Detailed designing concepts are shown in Figures S27 and S28.

Please cite this article in press as: Ma et al., Sequence spinning axially encoded metafibers, Matter (2023), https://doi.org/10.1016/j.matt.2023.08.006



enables large-scale preparation of rationally designed metafibers for further textile integration. We believe the metafiber provides an intriguing category of fiber materials to carry codes and promises a wide range of applications in smart textiles.

## EXPERIMENTAL PROCEDURES

### Resource availability

#### *Lead contact*

Further information and requests for resources and reagents should be directed to and will be fulfilled by the lead contact, Zhen Xu (zhenxu@zju.edu.cn).

#### *Materials availability*

This study did not generate new unique reagents.

#### *Data and code availability*

All the necessary data to evaluate the main conclusions of this paper have been shown in the main text and the supplemental information. Additional data related to the paper may be obtained from the authors upon request.

### Materials

Commercially available PU with different types (1170A and 3063D) was purchased from BASF (Ludwigshafen, Germany). Luminescent Nile red and coumarin were purchased from Hangzhou Bangyi Chemical. Polystyrene, polymethyl methacrylate, polyvinylidene fluoride (average Mw = 400,000), polyacrylonitrile (average Mw = 150,000), sodium alginate, and carboxymethyl cellulose were obtained from Aladdin. Polyacrylamide (average Mw = 15,000,000) and sodium polyacrylate (average Mw = 30,000,000) were purchased from Hangzhou Tongliyuan and Shanghai Yuanye Bio-Technology, respectively. $TiO_2$ nanoparticles (25 nm), $SiO_2$ (15 nm), and $Fe_3O_4$ (20 nm) were purchased from Aladdin. Graphene nanosheets was obtained from Nanjing XFNANO Materials Technology. Aqueous GO solution (1 wt %) with an average lateral size of 10–20 μm was purchased from Hangzhou Gaoxi Technology.

### Program-controlled MSS

Typically, the spinning dopes were DMF solutions of PU, and water was used as the coagulation bath. Firstly, we designed "Y"-shaped glass microchips. A controller (16 channel, Fluidiclab) was adopted to automatically control the solenoid valves (MTV-2-M6, Takasago) under the instruction of computer programs. Since the shifting of the solenoid valves will result in the turbulence of liquid flow, we used check valves (SS-11, Xiongchuan) to avoid turbulence and reflux. During the MSS process, the syringe dopes were injected into the valves under the pumping of syringe pumps (LSP01-2A). The spinning dopes were selectively introduced into the microchip under the instructions of the controller. Finally, the axially encoded metafibers solidified in a coagulation bath, followed by collection.

### Permutation arrangement of multicolor sequence metafibers

Firstly, 20 g PU pellets were added into 80 mL DMF at 80°C under vigorous stirring to form a homogeneous solution (20 wt %). We prepared spinning dopes with different colors by simply introducing commercial acrylic pigments into the PU solution. We designed a spinning program to control the solenoid valves according to the required color sequences. In the spinning process, the valve of the designed sequence was turned on while the other valves were kept off. The encoding was realized by shifting the state of the valves following the designed program. In a minimal

encoded unit, the possible categories of the metafibers (without code duplication) were calculated as

$$N = \begin{cases} n, (m = 1) \\ \frac{1}{2} C_n^m A_n^n, (m > 1) \end{cases}, \quad \text{(Equation 3)}$$

where N is the minimal unit type and n and *m* stand for the number of materials (codes) and sequences in the minimal unit (n > *m*), respectively. The color of the sequence was characterized by ImageJ using gray-value analysis of RGB channels.

### Encoding and decoding information in metafibers

In a long metafiber, the possible arrangement is an exponential function,

$$N = n^m, \quad \text{(Equation 4)}$$

where N is the metafiber type and n and m stand for the number of materials (codes) and sequences, respectively. For simplicity, we used two kinds of spinning dopes (n = 2) to encode information in the metafiber. We used $TiO_2$-hybrid PU ($TiO_2$:PU = 1:4) as the high-gray-value sequences (set as "0") and graphene-hybrid PU (graphene:PU = 1:4) as low-gray-value sequences (set as "1"). The digital information was firstly converted to a program, which was further used to control the sequence spinning. The decoding process of the obtained encoded metafibers was conducted by a brightness analysis on ImageJ. The high-gray-value sequences with programmed length were read as "0," and low-gray-value regions were read as "1."

### Fabrication of multimorphology metafibers

For the preparation of multimorphology metafibers, we designed two types of spinning dopes with different PU content (20 wt %, labeled as blue, and 5 wt %, labeled as yellow). We designed the spindle-shaped metafibers by alternatively encoding the two spinning dopes, and then the solidified metafibers were fixed at both ends for drying. The spindle was formed because of the axial solid content variation. For the sickle-shaped metafiber, we opened the valves of the 5 wt % PU dopes throughout the spinning process and encoded the 20 wt % PU dopes periodically.

### Fabrication of multihybrid metafibers

We prepared spinning dopes of $TiO_2$-hybrid PU (PU:$TiO_2$ = 10:1, labeled as blue) and $SiO_2$-hybrid PU (PU:$SiO_2$ = 10:1, labeled as yellow) by adding corresponding nanoparticles into PU solutions (20 wt %). Then, the solutions were used as the spinning dopes in the MSS as described before.

### Fabrication of multimaterial metafibers

We designed a library of multimaterial metafibers (Table S1). Spinning dopes of different materials (labeled with pigments for tagging) were encoded by MSS to realize the material variation along the fiber axial direction. Notably, the solvent was the best solvent of all encoded materials to prevent clogging in microchip, and the coagulation bath was the worst solvent of all materials to ensure solidification.

### Fabrication of mechano-metafibers

For the preparation of mechano-metafibers, TPU 3063D and 1070A were chosen as the stiff and soft sequences, respectively. To distinguish the stiff and soft sequences, TPU 3063D solution (20 wt %) was labeled as blue, and 1070A solution (20 wt %) was labeled as yellow. Then, the solutions were used as the spinning dopes in the MSS to fabricate the mechano-metafiber.

Please cite this article in press as: Ma et al., Sequence spinning axially encoded metafibers, Matter (2023), https://doi.org/10.1016/j.matt.2023.08.006



### Fabrication of electro-metafibers

To design conductive sequences (graphene-hybrid PU), graphene sheets were firstly dispersed in DMF by sonication (400 W, 24 h) and added to the PU solution (PU:graphene = 4:1). The neat PU solution was chosen to encode insulating sequences. Then, the solutions were used as spinning dopes in MSS to fabricate the electro-metafiber.

### Fabrication of magnetic metafibers

Two kinds of magnetic solutions were prepared by adding $Fe_3O_4$ (ferromagnetic) and $Al_2O_3$ (diamagnetic) to PU solutions (PU:$Fe_3O_4$ = 4:1, PU:$Al_2O_3$ = 4:1), respectively. Then, the solutions were used as spinning dopes in MSS to fabricate the magnetic metafiber.

### Fabrication of photothermo-metafibers

Two kinds of solutions were prepared by adding graphene (IR absorption) and $TiO_2$ (IR reflection) to PU solutions (PU:graphene = 4:1, PU:$TiO_2$ = 4:1), respectively. Then, the solutions were used as spinning dopes in MSS to fabricate the photothermo-metafiber.

### Characterizations

Luminescent sequences of axially encoded metafibers were measured on a high-resolution confocal microscope (LSM 880 with AiryScan). SEM images and energy-dispersive spectroscopy (EDS) measurements were taken on a Hitachi S4800 field-emission system. Electrical conductivity was conducted on a source meter (Keithley-2400). The magnetization curves of each sequence (cutoff) were taken on a magnetic property measurement system (MPMS-XL-5). IR reflectivity of PU/graphene and PU/$TiO_2$ was measured by a spectrometer (Nicolet iS50). The localized photothermal property of the metafibers was carried out on an IR pyrometer (FLIR T630sc). Tensile tests were carried out on an INSTRON (LEGEND-2344) instrument. Axial tensile modulus was measured by local tensile test with a gauge length of 5 mm. To study the local strain engineering of the mechano-metafibers, we used a digital camera to capture the deformation under tensile experiment, and the localized strain was calculated as

$$\varepsilon = \frac{\Delta l}{l} \times 100\% \qquad \text{(Equation 5)}$$

where $\varepsilon$ is the localized strain and $l$ and $\Delta l$ are the gauge length and increased length of the measured sequence, respectively.

## SUPPLEMENTAL INFORMATION

Supplemental information can be found online at https://doi.org/10.1016/j.matt.2023.08.006.

## ACKNOWLEDGMENTS

This work is supported by the National Natural Science Foundation of China (nos. 52122301, 51973191, 52090030, 51533008, 52272046, and 11890674); the Hundred Talents Program of Zhejiang University (188020*194231701/113); the Open Fund of Key Laboratory for Intelligent Nano Materials and Devices of the Ministry of Education (INMD-2020M05); the Fundamental Research Funds for the Central Universities (no. K20200060, 2021FZZX001-17, 2017QNA4036, and 2017XZZX001-04); and the Shanxi-Zheda Institute of New Materials and Chemical Engineering (nos. 2022SZ-TD012, 2022SZ-TD011, and 2021SZ-FR004).

## AUTHOR CONTRIBUTIONS

Z.X. and J.M. conceived the research and designed experiments. J.M. conducted the experiments, analyzed the data, and wrote the manuscript. Z.X. revised the manuscript. Z.X., Y.L., and C.G. supervised the project.

## DECLARATION OF INTERESTS

The authors declare no competing interests.

Received: May 29, 2023
Revised: July 15, 2023
Accepted: August 7, 2023
Published: August 28, 2023

## REFERENCES

1. Chen, C., Feng, J., Li, J., Guo, Y., Shi, X., and Peng, H. (2023). Functional fiber materials to smart fiber devices. Chem. Rev. *123*, 613–662.
2. Libanori, A., Chen, G., Zhao, X., Zhou, Y., and Chen, J. (2022). Smart textiles for personalized healthcare. Nat. Electron. *5*, 142–156.
3. Yang, Q., Yang, S., Qiu, P., Peng, L., Wei, T.R., Zhang, Z., Shi, X., and Chen, L. (2022). Flexible thermoelectrics based on ductile semiconductors. Science *377*, 854–858.
4. Maziz, A., Concas, A., Khaldi, A., Stålhand, J., Persson, N.K., and Jager, E.W.H. (2017). Knitting and weaving artificial muscles. Sci. Adv. *3*, e1600327.
5. Yan, W., Page, A., Nguyen-Dang, T., Qu, Y., Sordo, F., Wei, L., and Sorin, F. (2019). Advanced multimaterial electronic and optoelectronic fibers and textiles. Adv. Mater. *31*, 1802348.
6. Tuniz, A., Kaltenecker, K.J., Fischer, B.M., Walther, M., Fleming, S.C., Argyros, A., and Kuhlmey, B.T. (2013). Metamaterial fibres for subdiffraction imaging and focusing at terahertz frequencies over optically long distances. Nat. Commun. *4*, 2706.
7. Bai, H., Li, S., Barreiros, J., Tu, Y., Pollock, C.R., and Shepherd, R.F. (2020). Stretchable distributed fiber-optic sensors. Science *370*, 848–852.
8. Zheng, L., Zhu, M., Wu, B., Li, Z., Sun, S., and Wu, P. (2021). Conductance-stable liquid metal sheath-core microfibers for stretchy smart fabrics and self-powered sensing. Sci. Adv. *7*, eabg4041.
9. Lee, J., Ihle, S.J., Pellegrino, G.S., Kim, H., Yea, J., Jeon, C.Y., Son, H.C., Jin, C., Eberli, D., Schmid, F., et al. (2021). Stretchable and suturable fibre sensors for wireless monitoring of connective tissue strain. Nat. Electron. *4*, 291–301.
10. Yan, W., Noel, G., Loke, G., Meiklejohn, E., Khudiyev, T., Marion, J., Rui, G., Lin, J., Cherston, J., Sahasrabudhe, A., et al. (2022). Single fibre enables acoustic fabrics via nanometre-scale vibrations. Nature *603*, 616–623.
11. Bayindir, M., Abouraddy, A., Arnold, J., Joannopoulos, J., and Fink, Y. (2006). Thermal-sensing fiber devices by multimaterial codrawing. Adv. Mater. *18*, 845–849.
12. Liu, Z., Qi, D., Hu, G., Wang, H., Jiang, Y., Chen, G., Luo, Y., Loh, X.J., Liedberg, B., and Chen, X. (2018). Surface strain redistribution on structured microfibers to enhance sensitivity of fiber-shaped stretchable strain sensors. Adv. Mater. *30*, 1704229.
13. Chen, M., Wang, Z., Zhang, Q., Wang, Z., Liu, W., Chen, M., and Wei, L. (2021). Self-powered multifunctional sensing based on super-elastic fibers by soluble-core thermal drawing. Nat. Commun. *12*, 1416.
14. Chen, G., Li, Y., Bick, M., and Chen, J. (2020). Smart textiles for electricity generation. Chem. Rev. *120*, 3668–3720.
15. Chen, D., Jiang, K., Huang, T., and Shen, G. (2020). Recent advances in fiber supercapacitors: materials, device configurations, and applications. Adv. Mater. *32*, 1901806.
16. Liao, M., Wang, C., Hong, Y., Zhang, Y., Cheng, X., Sun, H., Huang, X., Ye, L., Wu, J., Shi, X., et al. (2022). Industrial scale production of fibre batteries by a solution-extrusion method. Nat. Nanotechnol. *17*, 372–377.
17. He, J., Lu, C., Jiang, H., Han, F., Shi, X., Wu, J., Wang, L., Chen, T., Wang, J., Zhang, Y., et al. (2021). Scalable production of high-performing woven lithium-ion fibre batteries. Nature *597*, 57–63.
18. Mo, F., Liang, G., Huang, Z., Li, H., Wang, D., and Zhi, C. (2020). An overview of fiber-shaped batteries with a focus on multifunctionality, scalability, and technical difficulties. Adv. Mater. *32*, 1902151.
19. Wang, L., Fu, X., He, J., Shi, X., Chen, T., Chen, P., Wang, B., and Peng, H. (2020). Application challenges in fiber and textile electronics. Adv. Mater. *32*, 1901971.
20. Shi, X., Zuo, Y., Zhai, P., Shen, J., Yang, Y., Gao, Z., Liao, M., Wu, J., Wang, J., Xu, X., et al. (2021). Large-area display textiles integrated with functional systems. Nature *591*, 240–245.
21. Zhang, Z., Guo, K., Li, Y., Li, X., Guan, G., Li, H., Luo, Y., Zhao, F., Zhang, Q., Wei, B., et al. (2015). A colour-tunable, weavable fibre-shaped polymer light-emitting electrochemical cell. Nat. Photonics *9*, 233–238.
22. Bayindir, M., Sorin, F., Abouraddy, A.F., Viens, J., Hart, S.D., Joannopoulos, J.D., and Fink, Y. (2004). Metal-insulator-semiconductor optoelectronic fibres. Nature *431*, 826–829.
23. Loke, G., Yuan, R., Rein, M., Khudiyev, T., Jain, Y., Joannopoulos, J., and Fink, Y. (2019). Structured multimaterial filaments for 3D printing of optoelectronics. Nat. Commun. *10*, 4010.
24. Rein, M., Favrod, V.D., Hou, C., Khudiyev, T., Stolyarov, A., Cox, J., Chung, C.C., Chhav, C., Ellis, M., Joannopoulos, J., and Fink, Y. (2018). Diode fibres for fabric-based optical communications. Nature *560*, 214–218.
25. Loke, G., Khudiyev, T., Wang, B., Fu, S., Payra, S., Shaoul, Y., Fung, J., Chatziveroglou, I., Chou, P.W., Chinn, I., et al. (2021). Digital electronics in fibres enable fabric-based machine-learning inference. Nat. Commun. *12*, 3317.
26. Xu, X., Zhou, X., Wang, T., Shi, X., Liu, Y., Zuo, Y., Xu, L., Wang, M., Hu, X., Yang, X., et al. (2020). Robust DNA-bridged memristor for textile chips. Angew. Chem. Int. Ed. Engl. *59*, 12762–12768.
27. Jiang, S., Liu, X., Liu, J., Ye, D., Duan, Y., Li, K., Yin, Z., and Huang, Y. (2022). Flexible metamaterial electronics. Adv. Mater. *34*, 2200070.
28. Qi, J., Chen, Z., Jiang, P., Hu, W., Wang, Y., Zhao, Z., Cao, X., Zhang, S., Tao, R., Li, Y., and Fang, D. (2022). Recent progress in active mechanical metamaterials and construction principles. Adv. Sci. *9*, 2102662.
29. Xu, L.L., Wang, C.F., and Chen, S. (2014). Microarrays formed by microfluidic spinning as multidimensional microreactors. Angew. Chem. Int. Ed. Engl. *53*, 3988–3992.
30. Gumennik, A., Wei, L., Lestoquoy, G., Stolyarov, A.M., Jia, X., Rekemeyer, P.H., Smith, M.J., Liang, X., Grena, B.J.B., Johnson, S.G., et al. (2013). Silicon-in-silica spheres via axial thermal gradient in-fibre capillary instabilities. Nat. Commun. *4*, 2216.
31. Kaufman, J.J., Tao, G., Shabahang, S., Banaei, E.H., Deng, D.S., Liang, X., Johnson, S.G., Fink,

Y., and Abouraddy, A.F. (2012). Structured spheres generated by an in-fibre fluid instability. Nature *487*, 463–467.

32. Gumennik, A., Levy, E.C., Grena, B., Hou, C., Rein, M., Abouraddy, A.F., Joannopoulos, J.D., and Fink, Y. (2017). Confined in-fiber solidification and structural control of silicon and silicon-germanium microparticles. Proc. Natl. Acad. Sci. USA *114*, 7240–7245.

33. Yu, Y., Wen, H., Ma, J., Lykkemark, S., Xu, H., and Qin, J. (2014). Flexible fabrication of biomimetic bamboo-like hybrid microfibers. Adv. Mater. *26*, 2494–2499.

34. Meng, Z.J., Zhang, J., Deng, X., Liu, J., Yu, Z., and Abell, C. (2019). Bioinspired hydrogel microfibres colour-encoded with colloidal crystals. Mater. Horiz. *6*, 1938–1943.

35. Huang, Q., He, F., Yu, J., Zhang, J., Du, X., Li, Q., Wang, G., Yu, Z., and Chen, S. (2021). Microfluidic spinning-induced heterotypic bead-on-string fibers for dual-cargo release and wound healing. J. Mater. Chem. B *9*, 2727–2735.

36. Du, X.Y., Li, Q., Wu, G., and Chen, S. (2019). Multifunctional micro/nanoscale fibers based on microfluidic spinning technology. Adv. Mater. *31*, 1903733.

37. Zhang, M., Wang, S., Zhu, Y., Zhu, Z., Si, T., and Xu, R.X. (2021). Programmable dynamic interfacial spinning of bioinspired microfibers with volumetric encoding. Mater. Horiz. *8*, 1756–1768.

38. Maisto, A., McDowall, D., Adams, D.J., and Del Giudice, F. (2023). Continuous manufacturing of microfluidic fibers embedded with ordered microparticles via ionic gelation. ACS Appl. Eng. Mater. *1*, 258–267.

39. Wang, H., Liu, H., Zhang, X., Wang, Y., Zhao, M., Chen, W., and Qin, J. (2021). One-step generation of aqueous-droplet-filled hydrogel fibers as organoid carriers using an all-in-water microfluidic system. ACS Appl. Mater. Interfaces *13*, 3199–3208.

40. Kang, E., Jeong, G.S., Choi, Y.Y., Lee, K.H., Khademhosseini, A., and Lee, S.H. (2011). Digitally tunable physicochemical coding of material composition and topography in continuous microfibres. Nat. Mater. *10*, 877–883.

41. Cho, S., Shim, T.S., and Yang, S.M. (2012). High-throughput optofluidic platforms for mosaicked microfibers toward multiplex analysis of biomolecules. Lab Chip *12*, 3676–3679.

42. Jang, K.I., Chung, H.U., Xu, S., Lee, C.H., Luan, H., Jeong, J., Cheng, H., Kim, G.T., Han, S.Y., Lee, J.W., et al. (2015). Soft network composite materials with deterministic and bio-inspired designs. Nat. Commun. *6*, 6566.

43. Ware, T.H., Biggins, J.S., Shick, A.F., Warner, M., and White, T.J. (2016). Localized soft elasticity in liquid crystal elastomers. Nat. Commun. *7*, 10781.

44. Erb, R.M., Sander, J.S., Grisch, R., and Studart, A.R. (2013). Self-shaping composites with programmable bioinspired microstructures. Nat. Commun. *4*, 1712.

45. Rylski, A.K., Cater, H.L., Mason, K.S., Allen, M.J., Arrowood, A.J., Freeman, B.D., Sanoja, G.E., and Page, Z.A. (2022). Polymeric multimaterials by photochemical patterning of crystallinity. Science *378*, 211–215.

46. Ma, J., Lin, S., Jiang, Y., Li, P., Zhang, H., Xu, Z., Wu, H., Lin, P., Breu, J., Gao, W., and Gao, C. (2020). Digital programming graphene oxide liquid crystalline hybrid hydrogel by shearing microlithography. ACS Nano *14*, 2336–2344.

47. Libanori, R., Erb, R.M., Reiser, A., Le Ferrand, H., Süess, M.J., Spolenak, R., and Studart, A.R. (2012). Stretchable heterogeneous composites with extreme mechanical gradients. Nat. Commun. *3*, 1265.

48. Ding, T., Chan, K.H., Zhou, Y., Wang, X.Q., Cheng, Y., Li, T., and Ho, G.W. (2020). Scalable thermoelectric fibers for multifunctional textile-electronics. Nat. Commun. *11*, 6006.

49. Alapan, Y., Karacakol, A.C., Guzelhan, S.N., Isik, I., and Sitti, M. (2020). Reprogrammable shape morphing of magnetic soft machines. Sci. Adv. *6*, eabc6414.

50. Ze, Q., Kuang, X., Wu, S., Wong, J., Montgomery, S.M., Zhang, R., Kovitz, J.M., Yang, F., Qi, H.J., and Zhao, R. (2020). Magnetic shape memory polymers with integrated multifunctional shape manipulation. Adv. Mater. *32*, 1906657.